Mouse-adapted MERS coronavirus causes lethal lung disease in human DPP4 knockin mice

Kun Li[a], Christine L. Wohlford-Lenane[a], Rudragouda Channappanavar[b], Jung-Eun Park[c], James T. Earnest[c], Thomas B. Bair[d], Amber M. Bates[e], Kim A. Brogden[e], Heather A. Flaherty[f], Tom Gallagher[c], David K. Meyerholz[g], Stanley Perlman[a,b], and Paul B. McCray Jr.[a,b,1]

[a]Department of Pediatrics, Pappajohn Biomedical Institute, University of Iowa, Iowa City, IA 52242; [b]Department of Microbiology, University of Iowa, Iowa City, IA 52242; [c]Department of Microbiology and Immunology, Loyola University Chicago, Maywood, IL 60153; [d]Iowa Institute of Human Genetics, University of Iowa, Iowa City, IA 52242; [e]College of Dentistry, University of Iowa, Iowa City, IA 52242; [f]Department of Veterinary Pathology, Iowa State University, Ames, IA 50011; and [g]Department of Pathology, University of Iowa, Iowa City, IA 52242

Edited by Diane E. Griffin, Johns Hopkins Bloomberg School of Public Health, Baltimore, MD, and approved March 2, 2017 (received for review November 21, 2016)

The Middle East respiratory syndrome (MERS) emerged in Saudi Arabia in 2012, caused by a zoonotically transmitted coronavirus (CoV). Over 1,900 cases have been reported to date, with ∼36% fatality rate. Lack of autopsies from MERS cases has hindered understanding of MERS-CoV pathogenesis. A small animal model that develops progressive pulmonary manifestations when infected with MERS-CoV would advance the field. As mice are restricted to infection at the level of DPP4, the MERS-CoV receptor, we generated mice with humanized exons 10–12 of the mouse *Dpp4* locus. Upon inoculation with MERS-CoV, human DPP4 knockin (KI) mice supported virus replication in the lungs, but developed no illness. After 30 serial passages through the lungs of KI mice, a mouse-adapted virus emerged ($MERS_{MA}$) that grew in lungs to over 100 times higher titers than the starting virus. A plaque-purified $MERS_{MA}$ clone caused weight loss and fatal infection. Virus antigen was observed in airway epithelia, pneumocytes, and macrophages. Pathologic findings included diffuse alveolar damage with pulmonary edema and hyaline membrane formation associated with accumulation of activated inflammatory monocyte–macrophages and neutrophils in the lungs. Relative to the parental MERS-CoV, $MERS_{MA}$ viruses contained 13–22 mutations, including several within the spike (S) glycoprotein gene. S-protein mutations sensitized viruses to entry-activating serine proteases and conferred more rapid entry kinetics. Recombinant $MERS_{MA}$ bearing mutant S proteins were more virulent than the parental virus in hDPP4 KI mice. The hDPP4 KI mouse and the $MERS_{MA}$ provide tools to investigate disease causes and develop new therapies.

emerging pathogen | interferon | virus pathogenesis | spike protein | CD26

Middle East respiratory syndrome (MERS) was recognized as a significant illness on the Saudi Arabian peninsula in mid-2012 and the causative agent was rapidly identified as a novel coronavirus (CoV) (1). MERS has a high mortality (∼36%) associated with severe lung disease that can progress to acute respiratory distress syndrome (ARDS). Since its emergence, the World Health Organization (WHO) has been notified of 1,905 laboratory-confirmed cases of MERS-CoV infection in 27 countries, resulting in at least 677 related deaths (WHO website, www.who.int/emergencies/mers-cov/en/; February 24, 2017). MERS-CoV, similar to the severe acute respiratory syndrome (SARS)-CoV that caused an epidemic in 2003, has been a serious cause for global concern due to its high fatality rate. Of note, the MERS-CoV has a genomic structure similar to that of other CoVs and contains a 30-kb positive-strand RNA genome that encodes for 11 ORFs that are ordered 5′ to 3′: ORF1a, ORF1b, spike (S), ORF3, ORF4a/b, ORF5, envelope (E), membrane (M), nucleocapsid (N), and ORF8b (1, 2). ORF1a and -1b are predicated to encode nonstructural proteins. The subgenomic mRNAs of MERS-CoV encode five unique accessory proteins, designated 3, 4a/b, 5, and 8b, which are found only in the virus lineage that includes HKU4 and HKU5 (1). Like other CoVs, the long genomic mRNA of MERS-CoV encodes replicase polyproteins that are further processed into multiple nonstructural proteins. In contrast, conserved S, E, M, and N structural proteins are translated from separate subgenomic mRNAs.

Epidemiologic studies have established that MERS is zoonotic in origin, with evidence for a closely related virus in dromedary camels on the Arabian Peninsula and throughout Africa (3–5). Spread from camels to people is documented (6), as is person-to-person spread among health care workers in hospital settings (7). The transmission of MERS-CoV from person to person is inefficient, but this could change with virus evolution (8, 9) and if the numbers of so-called "superspreaders" increased (10). The MERS-CoV has also been detected in people with mild, influenza-like illnesses, those with a dengue-like illness, and in those without obvious disease signs or symptoms (11–14). Although human-to-human or zoonotic spread of MERS has not reached epidemic or pandemic levels, its potential to spread between persons was demonstrated in healthcare settings in the Middle East (7) and by an outbreak in South Korea caused by a single infected individual (15).

A lack of autopsy studies from MERS fatalities has hindered understanding of MERS-CoV pathogenesis (16). None have been reported from Saudi Arabia or South Korea. To better understand the pathogenesis of MERS-CoV lung disease and aid the development of vaccines and therapies, we engineered a mouse model of MERS. Dipeptidyl peptidase 4 (DPP4, CD26), a type II transmembrane ectopeptidase, is the receptor for the MERS-CoV (17), and the key amino acids responsible for binding the virus

Significance

Middle East respiratory syndrome, caused by a zoonotically transmitted coronavirus (MERS-CoV), has a high mortality (∼36%). Because of limited autopsy data on tissues from MERS fatalities, a small animal model can provide an important tool to better understand the disease. We humanized the mouse locus of the virus receptor DPP4, preserving native DPP4 expression. After inoculating hDPP4 knockin mice with MERS-CoV, there was virus replication without disease. We then generated a mouse-adapted MERS-CoV by serial passage in hDPP4 knockin mice. The resultant virus causes fatal lung disease that includes diffuse alveolar damage and immune dysregulation. Here, we characterize the pathologic features of the model and elucidate key aspects of the immunopathology and factors contributing to virulence.

Author contributions: K.L., C.L.W.-L., R.C., T.G., S.P., and P.B.M. designed research; K.L., C.L.W.-L., R.C., J.-E.P., J.T.E., T.B.B., A.M.B., K.A.B., H.A.F., and D.K.M. performed research; K.L., C.L.W.-L., R.C., J.-E.P., J.T.E., T.B.B., H.A.F., T.G., D.K.M., S.P., and P.B.M. analyzed data; and K.L., T.G., S.P., and P.B.M. wrote the paper.

The authors declare no conflict of interest.

This article is a PNAS Direct Submission.

[1]To whom correspondence should be addressed. Email: paul-mccray@uiowa.edu.

This article contains supporting information online at www.pnas.org/lookup/suppl/doi:10.1073/pnas.1619109114/-/DCSupplemental.

spike glycoprotein have been identified (18). We replaced mouse *Dpp4* exons 10–12, encoding the residues required for virus binding, with human exons 10–12. In vivo serial passage of the human MERS-CoV [Erasmus Medical Center (EMC)/2012] in the human DPP4 receptor knockin (KI) mice yielded a mouse-adapted virus ($MERS_{MA}$) that causes a fatal pulmonary disease phenotype associated with diffuse alveolar damage and a severe inflammatory response, including an increased number of $CD11b^{+}$ $Ly6C^{hi}$ inflammatory monocyte–macrophages (IMMs). Sequencing of plaque-purified $MERS_{MA}$ clones revealed several mutations that emerged with in vivo passage, including a cluster in the spike (S) glycoprotein coding sequence. A recombinant MERS-CoV with these S-protein mutations was more virulent in DPP4 KI mice than parental MERS-CoV. The human DPP4 KI mouse infected with $MERS_{MA}$ revealed several important disease correlates, attributed to the virus and its cell entry, and to the host and its immunological response.

Results

Generation of a Mouse with Knockin of Human *DPP4* Exons 10–12. Whereas human *DPP4* has 26 exons, the residues encoded by exons 10–12 comprise the critical MERS-CoV receptor (18, 19). We and others showed previously that changing the exon 10–12 codons from mouse to human conferred high-affinity binding of the MERS S protein (20–23). Using a plasmid-mediated gene targeting strategy (*SI Appendix*, Fig. S1), a congenic C57BL/6 mouse was developed by replacing mouse *Dpp4* exons 10–12 with the corresponding human *DPP4* codons (hDPP4-KI). The targeted founders were expanded by breeding and offspring characterized by genotyping for the presence of human *DPP4* sequence as described in *Materials and Methods*. For the studies reported, we used mice homozygous for hDPP4. To identify the MERS-CoV receptor distribution in the mouse lung, we localized DPP4 in uninfected hDPP4-KI mice. As shown in Fig. 1*A*, airway epithelial cells had mild to moderate DPP4 immunoreactivity. In the alveolus, DPP4 immunostaining was most often seen in alveolar macrophages with less common immunostaining of alveolar epithelia, and the pleural surface (Fig. 1 *B* and *C*). This pattern of DPP4 expression shares similarities to the protein distribution in human lung (24, 25) and identifies cell types that may support virus replication.

Infection of Human *DPP4* Knockin Mice and Development of a Mouse-Adapted MERS-CoV. Following intranasal (i.n.) infection with 10^4 to 10^6 pfu MERS-CoV (EMC/2012, Vero 81 cell passaged, hereafter termed "EMC/Vero"), virus replicated in the lung (titers at 1 d.p.i. $\sim 10^{5-6}$ pfu/g tissue), but mice lost no weight and there was no mortality (Fig. 2 *A* and *B*). We next serially passaged EMC/Vero in KI mice as described in *Materials and Methods*. Tissue homogenates were saved after each in vivo passage. After 21 passages, we tested the passaged virus in KI mice and noted progressive weight loss and ~50% mortality (*SI Appendix*, Fig. S2). After 30 in vivo passages (P30), a 10^4 pfu virus inoculum caused progressive weight loss and ~80% mortality (Fig. 2 *A* and *B*). We termed this P30 virus mouse-adapted (MA) MERS-CoV or "$MERS_{MA}$."

Plaque-Purified $MERS_{MA}$ Causes Fatal Lung Disease in DPP4-KI Mice. Because CoV, like all RNA viruses, exist as quasispecies, we further purified $MERS_{MA}$ plaques. Six of nine plaque-purified isolates were evaluated in KI mice at a 10^5 pfu inoculum and each caused fatal disease (*SI Appendix*, Fig. S2). Serial passage of coronaviruses may result in gene deletions (26) and we observed that deletions had occurred in most of our plaques. Sequencing of the ORF3 and 4a/4b genes revealed that plaque 6 virions included a population without deletions in these regions (Dataset S1). Therefore, we selected virus from plaque 6 as a representative $MERS_{MA}$. To ensure complete clonal isolation, we performed two more rounds of plaque purification. Fig. 2 *C*–*F* shows that KI mice infected with a single triple plaque-purified virus, termed "clone 6.1.2," exhibited dose-dependent fatal disease. We compared the outcomes of male (Fig. 2 *C* and *D*) and female (Fig. 2 *E* and *F*) mice to several inocula of $MERS_{MA}$ clone 6.1.2 and observed similar outcomes. An inoculum of 5×10^3 pfu was lethal in both sexes.

Lung virus titers in KI mice infected with clone 6.1.2 were ~1–2 log higher compared with those challenged with the EMC/Vero parental virus from 1 to 5 days postinoculation (d.p.i.) (Fig. 3*A*). Virus was readily detected in serum of clone 6.1.2-infected mice, but rarely in mice infected with EMC/Vero (Fig. 3*B*). No virus was detected in the brain or other organs. We also examined viral RNA distribution by PCR and identified signal in lung at 1 and 3 d.p.i. (Fig. 3*C*). A low-level virus genomic RNA signal was also detected in the liver at 1 d.p.i. only. Of note, the EMC/Vero virus yielded more progeny than clone 6.1.2 virus in human cells (Fig. 3*D*), suggesting that mouse adaptation did not enhance infection in human cells.

We compared the tissue histology of KI mice infected with EMC/Vero or $MERS_{MA}$ clone 6.1.2. At 1 and 3 d.p.i. we noted similar mild inflammatory cell infiltrates in perivascular regions and alveolar septa of mice infected with both viruses. By 4 and 5 d.p.i., lung tissue from mice infected with EMC/Vero virus was notable for multifocal mononuclear cell infiltrates (Fig. 4*A*, arrowheads), whereas such infiltrates were mild and uncommon in the clone 6.1.2-infected animals. In contrast, tissues from clone 6.1.2-infected mice showed multifocal hyaline membranes (Fig. 4 *A* and *B*, black arrows), edema (Fig. 4*B*, black asterisks), and necrotic debris (Fig. 4*B*, *Inset*, red arrowhead) consistent with diffuse alveolar damage. Associated with these findings in clone 6.1.2-infected animals, we observed Evans blue dye retention in lung tissue at 4 and 5 d.p.i., indicative of increased vascular permeability (Fig. 4*B*, white asterisks). Morphometric analysis of lung tissue lesions showed that clone 6.1.2-infected lungs had significantly reduced cellular infiltrates and increased hyaline membranes at 4 and 5 d.p.i. (Fig. 4*C*). We localized virus N protein in infected lung tissue at 3 d.p.i. In EMC/Vero-infected mice, virus antigen staining was patchy and featured immunostaining of alveolar macrophages and less common staining of alveolar and airway epithelia (Fig. 5, *Middle*). In contrast, clone 6.1.2-infected mice had much more widespread N-protein staining of alveolar macrophages and alveolar epithelia

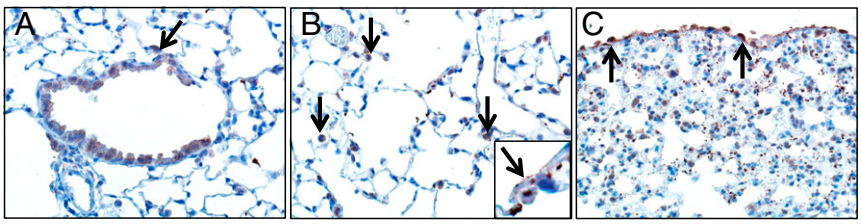

Fig. 1. DPP4 immunostaining in uninfected hDPP4 KI mouse lung. (*A*) DPP4 was observed as mild to moderate cytoplasmic staining of airway epithelia. Positive staining was also noted in alveolar macrophages (arrow). (*B*) Mild to moderate macrophage immunostaining were commonly seen (arrows, *Middle*), as was weak staining of alveolar epithelia (*Inset*). (*C*) The pleural surface (arrows) had multifocal DPP4 immunostaining. Results shown are representative of findings from four hDPP4 KI mice. (Magnification: 400×.)

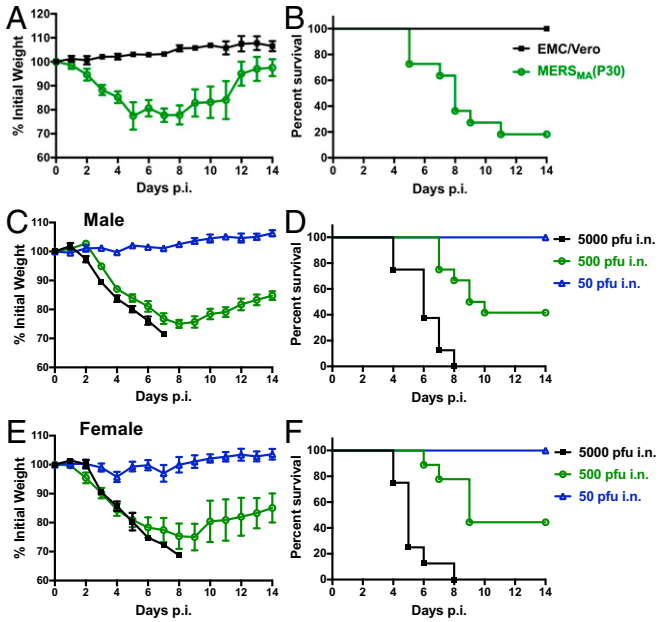

Fig. 2. Outcomes in hDPP4 KI mice infected with EMC/Vero or MERS$_{MA}$. Weight loss (*A*) and survival (*B*) in KI mice infected i.n. with 10^4 pfu EMC/Vero or passage 30 (P30) MERS$_{MA}$. EMC/Vero-infected mice had 100% survival. Human DPP4 KI mice infected with P30 MERS$_{MA}$ lost significant weight and most died. Results summarize two replicate experiments, $n = 10$ (EMC/Vero), $n = 11$ (MERS$_{MA}$), mixed male and female mice. (*C*–*F*) MERS$_{MA}$ clone 6.1.2 causes dose-dependent lethal lung disease in male and female hDPP4 KI mice. (*C* and *D*) Weight curve and survival results for male hDPP4 KI mice that received 5,000–50 pfu MERS$_{MA}$ clone 6.1.2 via i.n. inoculation. (For 5,000 pfu $n = 8$; 500 pfu $n = 12$; and 50 pfu $n = 5$). (*E* and *F*) Weight curve and survival results for female hDPP4 KI mice that received 5,000–50 pfu MERS$_{MA}$ clone 6.1.2 via i.n. inoculation. (For 5,000 pfu $n = 8$; 500 pfu $n = 9$; and 50 pfu $n = 5$). (*A*, *C*, and *E*) Data represent mean ± SE.

and scattered airway epithelia (Fig. 5, *Right*), consistent with the clinical and virological results.

Immune Response to MERS$_{MA}$. Studies of patients with MERS-CoV (27–29), infected animal models (30–33), and cultured cells (34–37) indicate that delayed IFN signaling and dysregulated cytokine and chemokine production may contribute to disease severity. We measured mRNA abundance for several antiviral and proinflammatory cytokines and chemokines, and IFN-stimulated genes (ISGs) in lung tissue from KI mice infected with EMC/Vero and clone 6.1.2, at 1 and 3 d.p.i. using qRT-PCR. As shown in *SI Appendix*, Fig. S3, the induction of several host defense genes was similar for both viruses. Among the transcripts expressed in greater abundance in response to clone 6.1.2 were the type I and III interferons and IL-6, IL-10, CCL2, CXCL10, and MDA5 at 3 d.p.i. (*SI Appendix*, Fig. S3). We also profiled the abundance of selected cytokine and chemokine proteins in serum and lung tissue homogenates at 3 d.p.i. (*SI Appendix*, Fig. S4). Notable differences between clone 6.1.2 and EMC/Vero included greater elevations in CCL2, CXCL2, IL-6, CXCL10, and G-CSF. Overall, the more virulent clone 6.1.2 elicited delayed, but ultimately greater, types I and III IFN-transcript responses and more robust cytokine/chemokine responses than the parental virus.

Analysis of peripheral blood smears collected at 4 d.p.i. revealed that MERS$_{MA}$ clone 6.1.2-infected mice had a greater percentage of neutrophils and fewer lymphocytes than EMC/Vero-infected mice (*SI Appendix*, Fig. S5*A*). Both EMC/Vero and clone 6.1.2-infected mice exhibited an increase in reactive lymphocytes (*SI Appendix*, Fig. S5*A*) consistent with response to infection. Peripheral blood from clone 6.1.2-infected mice also had morphologic evidence of monocyte activation, a reduced erythrocyte density, and reduced polychromatophils (immature RBCs) consistent with anemia of inflammation (*SI Appendix*, Fig. S5 *B* and *C*). These results provide further evidence of a systemic illness in clone 6.1.2-infected animals.

Examination of autopsy samples from patients who succumbed to SARS and MERS ($n = 1$) showed substantial accumulation of monocyte–macrophages and neutrophils in the lungs (38–41). To determine whether the enhanced morbidity and mortality of hDPP4-KI mice to MERS$_{MA}$ clone 6.1.2 infection correlated with increased inflammatory cell recruitment, we analyzed the percentages and total numbers of innate immune cell populations in the lungs at 4 d.p.i. Whereas the absolute numbers of CD45$^+$ leukocytes were lower in clone 6.1.2-challenged mice, percentages and total numbers of CD11b$^+$ Ly6C^{hi} IMMs were significantly higher in clone 6.1.2-infected mice compared with EMC/Vero-infected or uninfected control mice (Fig. 6 *A* and *B*). In contrast, neutrophil numbers were variable and not statistically different between groups (Fig. 6 *A* and *B*). Staining for activation markers (CD69 and CD80) revealed that IMMs and neutrophils were highly activated in clone 6.1.2-infected mice and less so in EMC/Vero-infected mice (Fig. 6 *C* and *D*). IMM and neutrophil activation was significantly lower in uninfected control mice compared with the two groups of infected mice (Fig. 6 *C* and *D*). We next enumerated NK-, T-, and B-cell numbers in the lungs of the different groups and observed higher numbers in EMC/Vero-infected mice compared with clone 6.1.2-infected or uninfected mice (Fig. 6*E*). In summary, whereas substantially more mononuclear cells were detected in EMC/Vero compared with MERS$_{MA}$ clone 6.1.2-infected lungs, the infitrates were composed mainly of lymphocytes in the former group. Conversely, more IMMs and fewer lymphocytes were detected in the lungs of animals infected with clone 6.1.2 compared with EMC/Vero virus. Overall, the increased accumulation of activated monocyte–macrophages and neutrophils and decreased numbers of T and B cells in the lungs of MERS$_{MA}$ clone 6.1.2-challenged mice

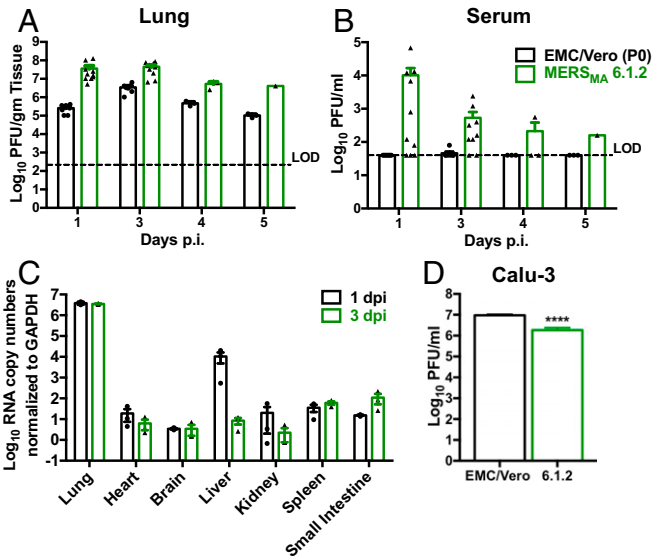

Fig. 3. Tissue virus titers and viral genomic RNA distribution. Human DPP4 KI mice infected with 10^4 pfu i.n. inoculum of indicated MERS-CoV. (*A* and *B*) Lung and serum titers at indicated times (*C*) ORF1a quantitative RT-PCR performed on indicated tissues from EMC/Vero and MERS$_{MA}$ clone 6.1.2-infected mice at 1 and 3 d.p.i. Limit of detection (LOD) for qRT-PCR assay is ~100 copies. Mean ± SE; $n = 3$. (*D*) Calu-3 cells were infected with indicated MERS-CoV at MOI 0.1 and virus titers at 1 d.p.i were determined by plaque assay. $n = 6$, representative of two replicate experiments. Statistical significance was assessed by Student's *t* test. ****$P < 0.0001$.

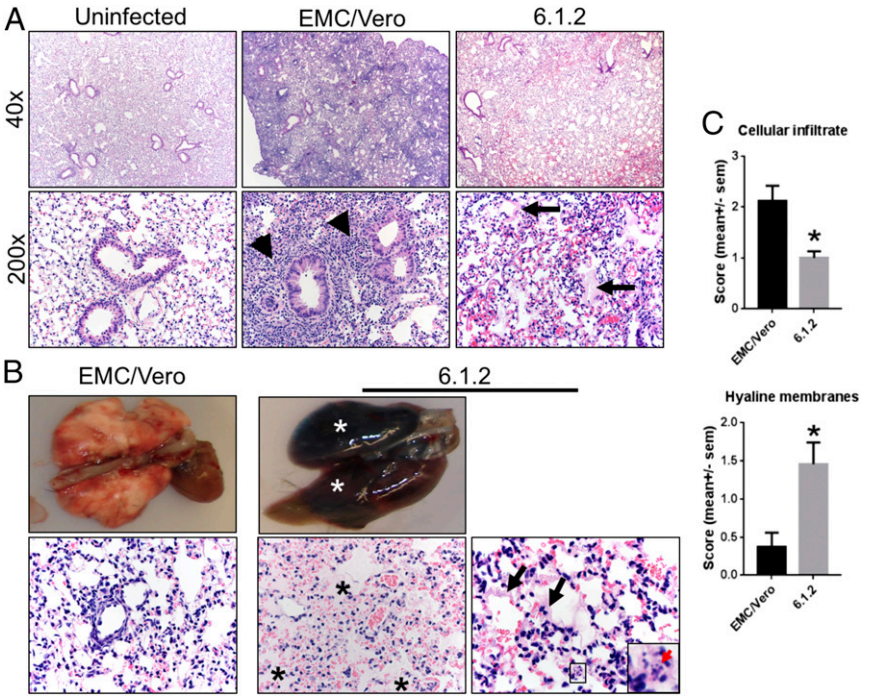

Fig. 4. Lung pathology and scoring at days 4–5 postinfection. (*A*) The uninfected group lacked lesions. EMC/Vero virus infection was characterized by multifocal mononuclear infiltrates (arrowheads), but mononuclear infiltrates were mild and uncommon in the clone 6.1.2-infected group. Rather, clone 6.1.2-infected lungs were characterized by multifocal hyaline membranes (*A*, arrows), edema, and necrotic debris that was consistent with diffuse alveolar disease: 40x (*Top*) and 200x (*Bottom*). (*B* and *C*) Further characterization of alveolar disease in EMC/Vero and clone 6.1.2 virus infection. Grossly (*B*, *Top* images), Evans blue dye (administered i.v. before killing) was not retained in EMC/Vero infection but was retained in clone 6.1.2 (white asterisks), indicative of vascular leakage. Histopathology (*B*, *Bottom* images) of EMC/Vero and clone 6.1.2 lungs. EMC/Vero-infected lung (*Left*) had perivascular to interstitial mononuclear infiltrates. Clone 6.1.2-infected lung exhibited edema (black asterisks, *Bottom Middle*, 400x), scattered cell death/debris (*Inset* and red arrow, *Bottom Right*), and/or hyaline membranes (black arrows, 600x). (*C*) Morphometry of lung tissues showed that clone 6.1.2 lungs had significantly reduced cellular infiltrate and increased hyaline membranes ($P = 0.01$ and $P = 0.003$, respectively, Mann–Whitney). $n = 5$–6 mice per condition.

suggest an overt and injurious innate inflammatory response and a suboptimal adaptive immune response.

Identification of MERS-CoV Mutations Acquired During Mouse Adaptation. To identify the changes fixed into MERS-CoV during serial passaging, we sequenced several mouse-adapted virus genomes using the Illumina MiSeq platform including: EMC/Vero (tissue culture passaged in Vero 81 cells), passage 21 $MERS_{MA}$, 9 plaques from passage 30 $MERS_{MA}$, and 6 triple plaque-purified $MERS_{MA}$ clones. Each sequenced $MERS_{MA}$ genome had between 12 and 21 nonsynonymous differences compared with the published EMC/2012 isolate (42). These differences are noted in *SI Appendix*, Fig. S5 and Dataset S1, in the context of MERS-CoV ORFs. EMC/Vero differed from EMC/2012 at three loci: NSP3

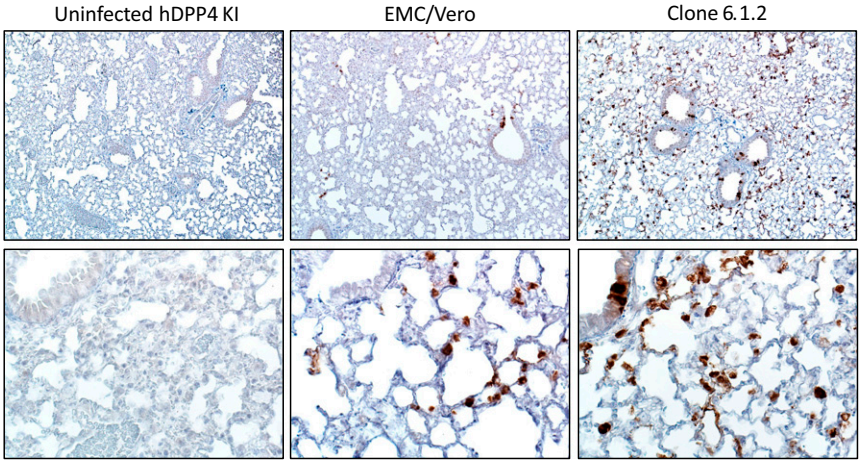

Fig. 5. MERS-CoV N-protein immunolocalization in uninfected KI mice or mice infected with EMC/Vero or $MERS_{MA}$ clone 6.1.2. No antigen staining was observed in uninfected hDPP4 KI mice (*Left*). At 3 d.p.i., mice infected with EMC/Vero had a patchy distribution of virus antigen (brown stain), including macrophage immunostaining along with uncommon epithelia of alveoli and airways (*Middle*). In contrast, clone 6.1.2-infected mice had widespread infection with staining of macrophages, alveolar epithelia, and scattered airway cells (*Right*). $n = 3$–4 mice per condition. [Magnification: 100x (*Top*) and 400x (*Bottom*.]

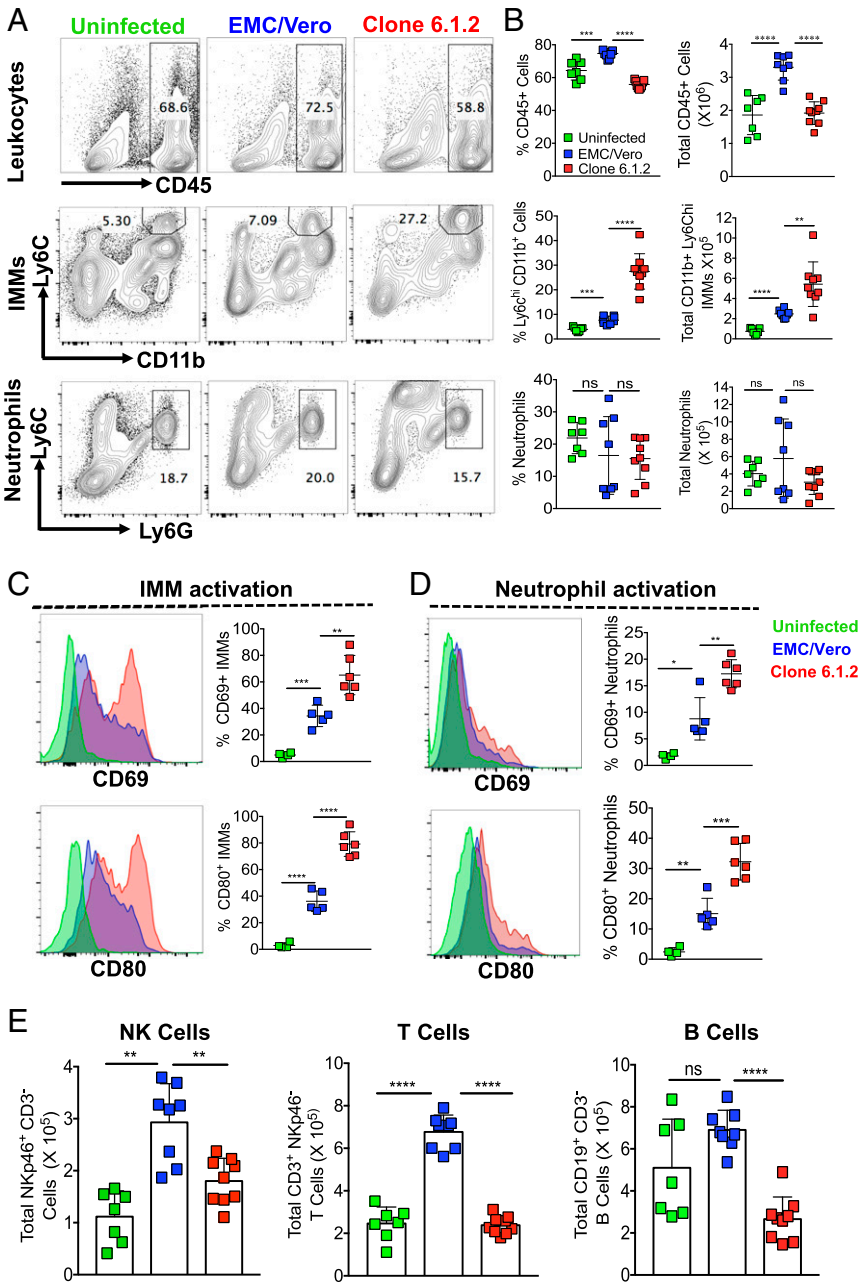

Fig. 6. Accumulation of activated innate immune cells in the lungs of clone 6.1.2-infected hDPP4 KI mice. Lungs harvested from uninfected hDPP4 KI mice or hDPP4 KI mice challenged with 1×10^4 pfu of EMC/Vero or MERS $_{MA}$ clone 6.1.2 were analyzed for infiltrating immune cells on day 4 p.i. (*A*) FACS plots (*Left*) show percentages of leukocytes, inflammatory monocyte–macrophages, and neutrophils in the lungs of uninfected, EMC/Vero, and clone 6.1.2 groups. (*B*) Scatterplots (*Right*) represent percentages and total numbers of immune cells in the lungs of uninfected, EMC/Vero, and clone 6.1.2 groups. (*C* and *D*) Histograms and scatterplots show levels of activation markers, CD69 and CD80 on lung-derived IMMs (*C*), and neutrophils (*D*). (*E*) Bar graphs with scatterplots show total number of NK, T, and B cells in the lungs of uninfected, EMC/Vero, and clone 6.1.2 groups. Data were derived from two independent experiments with three to six mice per group per experiment. $*P < 0.05$, $**P < 0.01$, $***P < 0.001$, $****P < 0.0001$.

(S1112F), spike (T1015N), and Orf5 (W108X). Missense mutations were present in all MERS$_{MA}$ isolates, including 13 in 1a/1b, 7 in S, 1 in 3, 1 in 4a, 2 in 4b, 1 in 5, 1 in M, and 2 in N. We also observed nonsense or frameshift mutations in ORF5 that arose during early Vero cell tissue culture amplification of the original EMC/2012 isolate. Interestingly, most clones encoded virus deleted in ORFs 3a, 3b and or 4, but clone 6.1.2 expressed full-length 3, 4a, and 4b gene products (*SI Appendix*, Fig. S6 and Dataset S1). We observed no evidence for differences in virulence when isolates containing ORF3/4a/4b or lacking their expression were compared (see passage 30 isolates in *SI Appendix*, Fig. S2 and Dataset S1). Compared with EMC/Vero, 6 unique mutations emerged in the S-protein coding sequence of MERS$_{MA}$ viruses. Every isolate had mutations in the S protein, including the passage 21 isolate, which was not fully virulent. Because variations in CoV S proteins frequently correlate with virulence (43, 44), we next assessed whether the S-protein changes accounted for the gain in virulence described above.

We noted that the virus that initiated the serial passages, EMC/Vero, differed from the prototype human isolate EMC/2012 at

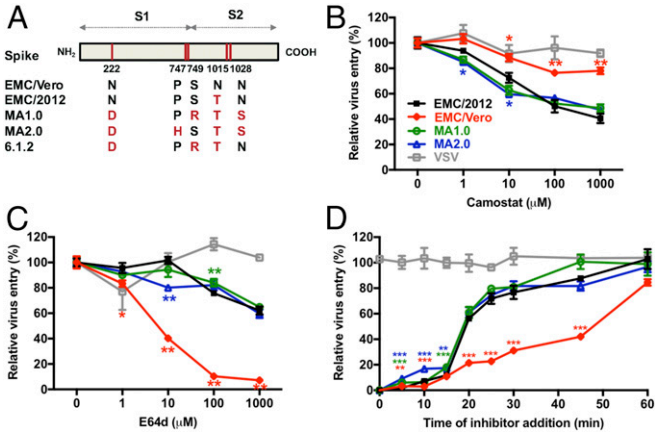

Fig. 7. Adapted mutations in spike protein influence virus entry. (*A*) Linear depiction of MERS-CoV S1 (receptor binding) and S2 (fusion) domains. Amino acid changes in EMC/2012 and mouse-adapted MERS-CoV S proteins (MA1.0 and MA2.0) are indicated relative to the parent virus EMC/Vero. (*B* and *C*) Effects of E64d and camostat on MERS pseudovirus entry into LET1 cells. (*D*) Kinetics of MERS pseudovirus entry into LET1 cells. Error bars represent mean ± SE $*P < 0.05$, $**P < 0.01$, $***P < 0.001$ compared with EMC/2012 S.

S residue 1015 (Fig. 7*A*). The EMC/Vero contained N1015, a residue reported in tissue culture adapted MERS-CoV (45). We observed a reversion of this residue during serial passage in KI mice, where N1015 returned to the T residue found in EMC/2012. On continued passage in KI mice, additional S mutations arose, notably the P747H and S749R residues comprising part of the S-proteolytic cleavage site. To gain insights into how these S mutations might contribute to virulence, we constructed a series of S genes reflecting EMC/Vero, EMC/2012, and those in $MERS_{MA}$ p30 (Fig. 7*A*). The constructs termed MA1.0 and MA2.0 featured S-protein mutations representative of all that arose during mouse adaptation, including those present in clone 6.1.2 (Fig. 7*A*). We evaluated the effect of these S mutations on cell entry using vesicular stomatitis virus-based MERS S pseudoviruses (46). These viruses were transduced into murine lung epithelial type I cells (47) expressing hDPP4 (48). Strikingly, we found that EMC/Vero S-directed cell entry was highly sensitive to the cysteine protease inhibitor E64d, which inactivates endosomal cathepsins, but relatively resistant to the serine protease inhibitor camostat, which inactivates cell-surface transmembrane proteases (Fig. 7 *B* and *C*). These findings indicated that the MA mutations, particularly the N1015T change, shifted viruses from using endosomal cathepsins, over to cell-surface transmembrane proteases. Cell-surface transmembrane proteases "trigger" a rapid virus–cell entry (46, 49). Consistently, the EMC/2012 and MA pseudoviruses entered cells with rapid kinetics, achieving 50% of maximal cell entry in 20 min. By contrast, the entry of EMC/Vero viruses were relatively slow, with less than 40% of maximal cell entry in 45 min (Fig. 7*D*). These results indicated that MERS-CoV spikes evolve in vivo for utilization of cell-surface transmembrane proteases, thereby accelerating cell entry and increasing productive infections in the mouse lung.

S-Protein Mutations in $MERS_{MA}$ Contribute to Virulence. To evaluate the effects of the evolved S-protein mutations on virulence, we used reverse genetics to introduce $MERS_{MA}$ S-gene mutations into an infectious MERS-CoV (EMC/2012 genome) bacterial artificial chromosome (pBAC-$MERS^{FL}$) as described in *Materials and Methods* (50, 51). Recombinant MERS-CoV were prepared bearing the S proteins from EMC/2012 (42) or mouse-adapted viruses (MA1.0, or MA2.0). The sequence-verified BACs were transfected into Huh7 cells to generate recombinant MERS-CoVs, which were then amplified in Calu3 cells to obtain stocks. The recombinant EMC/2012 MERS-CoV (42) and the MA1.0 and MA2.0 recombinants were inoculated into 12- to 18-wk male hDPP4-KI mice to assess disease outcomes and virus titers. Following a 10^4 pfu inoculum, the recombinant viruses caused a mild transient weight loss with no mortality (Fig. 8 *A* and *B*). At a higher 10^5 pfu inoculum, the MA1.0 and MA2.0 recombinant viruses caused greater weight loss than the recombinant EMC/2012 virus (42), with ~40% mortality in MA2.0-infected mice (Fig. 8 *C* and *D*). Lung tissue titers at 1 d.p.i. were slightly increased in the mice infected with the MA2.0 S protein at the 10^5 pfu inoculum (Fig. 8*E*). Of interest, these recombinant viruses caused minimal weight loss and no mortality in young 6- to 8-wk hDPP4-KI mice (*SI Appendix*, Fig. S7). The replication properties of these three recombinant viruses were similar in human Calu-3 and Huh7 cell lines (Fig. 8*F*), indicating that, whereas mutations arising in the S protein partially contribute to the increased virulence observed in $MERS_{MA}$-infected mice, they did not enhance growth in human cells.

Discussion

Whereas MERS represents an ongoing risk to human health, there has been only one postmortem study of a patient with MERS (16), and our knowledge of human disease pathophysiology is poor. To develop a more robust small animal model to study MERS pathogenesis, we generated hDPP4 knockin mice with exons 10–12 replaced by the human codons, retaining gene regulation by the native promoter. Although hDPP4-KI mice supported modest replication of EMC/Vero MERS-CoV in the lung, the

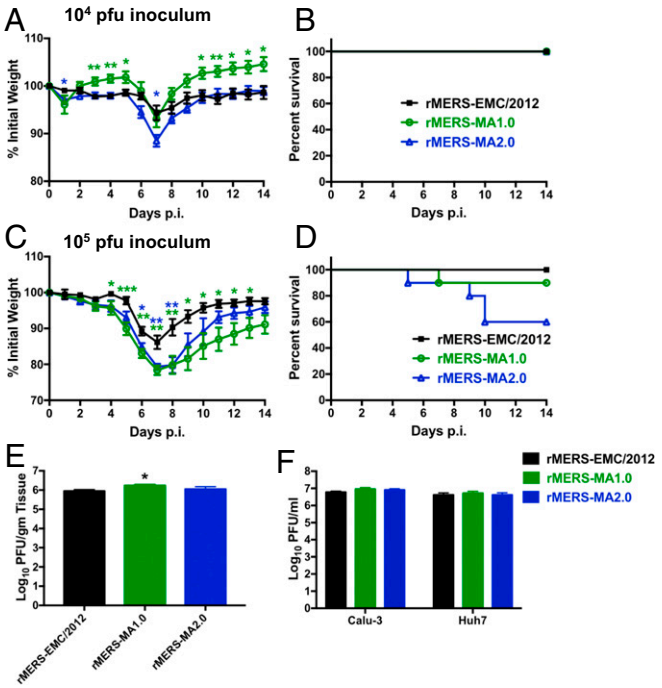

Fig. 8. Influence of adapted spike protein mutations on in vivo virulence. (*A* and *B*) KI mice (age 12–13 wk, male) received 10^4 pfu of indicated recombinant MERS-CoV and were monitored daily for weight (*A*) and mortality (*B*) (n = 8 per group, representative of two replicate experiments). (*C* and *D*) KI mice (age 12–18 wk, male) received 10^5 pfu of indicated recombinant MERS-CoV and were monitored daily for weight (*C*) and mortality (*D*) (n = 10 per group, representative of two replicate experiments). (*E*) Lung virus titers at 1 d.p.i. determined by plaque assay in animals that received the 10^5 pfu inoculum (n = 6 per group, representative of two replicate experiments). (*F*) Calu-3 and Huh7 cells were infected with indicated recombinant viruses at MOI = 0.1. Progeny were collected at 1 d.p.i. and titered by plaque assay. (n = 6, representative of two replicate experiments). Error bars represent mean ± SE $*P < 0.05$, $**P < 0.01$, $***P < 0.001$ compared with rMERS-CoV EMC/2012.

infection was largely asymptomatic. Thirty in vivo serial passages of EMC/Vero MERS-CoV in KI mice led to an evolved $MERS_{MA}$ strain that caused lethal pneumonia. Compared with the parental virus, $MERS_{MA}$ infection featured diffuse alveolar damage, dysregulated innate immune responses, and the presence of activated inflammatory monocyte–macrophages and neutrophils. Sequencing of $MERS_{MA}$ genomes revealed that mouse-adapted viruses developed mutations in several genes including the S protein. The virulent $MERS_{MA}$ clone 6.1.2 had 12 mutations in coding sequences and one mutation in a noncoding region of the virus genome. Studies of recombinant MERS-CoVs bearing these S-protein mutations showed that these viruses caused increased morbidity and mortality in adult KI mice. The hDPP4-KI mouse and the $MERS_{MA}$ provide tools to investigate disease pathogenesis and evaluate new therapies.

Comparison with Other Models of MERS-CoV Infection. Several animal species have been screened for their susceptibility to MERS-CoV infection. Mice (52), ferrets (53), and Syrian hamsters (54) do not support MERS-CoV replication. In contrast, the lungs of rhesus macaques (31, 55), marmosets (30), rabbits (56), and camels (57) are permissive to virus replication. Marmosets develop lung disease and associated mortality in response to a large inoculum (30), but others report minimal disease in marmosets (58). Overall the phenotypes in other mammals studied are mild and do not result in severe MERS-like disease. We reported a small animal model of MERS, the Ad-hDPP4 sensitized mouse (48), and subsequently we and others (33, 59) generated mice transgenic for hDPP4 using various promoters. When transgenic mice expressing hDPP4 under control of the cytokeratin 18 promoter (32) or a ubiquitous promoter (33) were exposed to MERS-CoV, they developed fatal disease, but lethality occurred after mice developed an overwhelming encephalitis.

Pascal et al. recently reported making a mouse with humanized *DPP4* exons using an alternative strategy (60). Following an inoculum of 2×10^5 pfu of human MERS-CoV isolates, these mice supported virus replication (10^6 to 10^7 pfu per gram of tissue), with histopathologic features of mild–moderate peribronchiolar inflammation, interstitial inflammation, and alveolar thickening observed at 2 and 4 d.p.i. Additional studies in this model demonstrated that a dosage of 2.5×10^4 pfu MERS-CoV caused ~20% weight loss, necessitating euthanasia. In these mice, depletion of $CD8^+$ T cells reduced disease severity, whereas macrophage depletion exacerbated MERS-CoV–induced lung pathology and disease signs (61), but whether $CD8^+$ T-cell or macrophage depletion would have the same effects in mice with lethal disease remains to be determined. In contrast, the human DPP4 knockin mouse infected with $MERS_{MA}$ reported here showed enhanced virus replication, significant lung pathology, and mortality with an inoculum as low as 5×10^2 pfu. These differences likely derive from the array of mutations that arose following 30 in vivo serial passages, including those in the S protein. While this manuscript was under review, Cockrell et al. reported engineering a MERS model by changing two amino acids in the mouse *Dpp4* locus (62). This innovation, combined with in vitro and in vivo serial passage, yielded a virulent mouse-adapted MERS-CoV with mutations distinct from those identified here, indicating that there are several evolutionary pathways to mouse virulence.

Comparison of MERS-CoV Disease in Human Lung and Human DPP4 Knockin Mice. The cell types susceptible to MERS-CoV infection in human lung were first identified in ex vivo studies and include nonciliated bronchial epithelial cells (17), as well as type I and II pneumocytes, endothelia, and fibroblasts (45). Investigators using human bronchial and lung tissue grown in ex vivo organ cultures observed infection of nonciliated bronchial epithelium, bronchiolar epithelial cells, alveolar epithelial cells, and endothelial cells (63) and detected morphological correlates of severe lung injury (64). The most severe manifestation of MERS in humans is a lethal pneumonic process with associated diffuse alveolar damage (2, 16). Autopsy results from a single individual that died from MERS were recently reported (16). Key histopathologic findings included MERS-CoV antigen localization in pneumocytes, macrophages, and endothelial cells with evidence of diffuse alveolar damage. No evidence of antigen staining was found in other organs (16). Similarly, $MERS_{MA}$ clone 6.1.2 infection in hDPP4 KI mice caused a predominantly parenchymal lung disease associated with diffuse alveolar damage, a common pathologic feature of ARDS.

A rapid and well-coordinated innate immune response is a first line of defense against viral infections, but dysregulated and excessive immune responses may cause immunopathology and increase morbidity and mortality (65–68). Although there is no direct evidence for the involvement of proinflammatory cytokines and chemokines in disease pathogenesis, correlative findings from patients with MERS with severe disease suggest a role for exuberant inflammatory responses in the disease process. MERS-CoV infection results in a delayed but elevated antiviral and proinflammatory cytokine and chemokine expression in dendritic cells, monocyte–macrophages, and epithelial cells (31, 34, 69). Additionally, studies in patients with MERS with varying disease severity showed higher virus titers and elevated levels of serum proinflammatory cytokines (IL-6 and IFN-α) and chemokines (IL-8, CXCL-10, and CCL5) in individuals with severe MERS compared with those with mild to moderate disease (28, 29, 70, 71). Similarly, mice infected with $MERS_{MA}$ clone 6.1.2 displayed high lung virus titers associated with a delay in the induction of IFN responses. Furthermore, elevated proinflammatory cytokines and the accumulation of activated monocyte–macrophages and neutrophils in the lung suggest a possible role for immunopathologic responses in the greater tissue injury and fatal pneumonia we observed.

Viral Mutations Associated with Adaptation to the Mouse Lung. Sequencing the genomes of $MERS_{MA}$ strains and triple plaque-purified clones from virulent strains identified several coding sequence mutations, including changes in the S protein. The S-protein mutations were not within the receptor binding domain. Rather, they arose in proteolytic substrate sites and in subdomains that control S-protein-catalyzed virus–cell membrane fusions. $MERS_{MA}$ clone 6.1.2 and the recombinant MA1.0 and MA2.0 viruses all exhibited S-protein mutations associated with "early entry" (46), a characteristic of coronaviruses that preferentially use cell-surface transmembrane proteases, such as TMPRSS2 (72, 73), for their virus–cell membrane fusion activation and resultant cell entry. We speculate that the mouse adapted viruses are selected on the basis of their utilization of these transmembrane proteases, which may be abundantly available in the mouse lung, but sparse on other settings, such as Vero cell cultures. The $MERS_{MA}$ clone 6.1.2 genome contained 10 additional missense mutations outside of the the S protein. Because the S-protein changes in isolation resulted in only a modest gain in virulence (Fig. 8), it will be important to determine which other mutations are also critical for the pathogenic changes that we observed. The mouse passage-associated mutations that arose in MERS-CoV nonstructural proteins may also contribute to virulence and evasion of the host immune response. Of note, at least one of them, nsp9, was also mutated in mouse-adapted SARS-CoV and contributes to increased virulence (74), although the function of this protein remains unknown.

Advantages and Limitations of the Mouse Model. The hDPP4 KI mouse model offers some advantages over previous small animal models for MERS-CoV disease. Unlike the Ad-hDPP4–sensitized mouse model, hDPP4 KI mice do not require a prior transduction process (48). In contrast to transgenic mice expressing hDPP4 by tissue-specific (32) or ubiquitous promoters (33, 59), hDPP4 KI mice do not develop brain disease. The model should be useful in studies of disease pathogenesis, vaccine applications, and evaluation

of small molecule inhibitors and other therapies. In addition, hDPP4 KI mice may be useful in modeling the comorbidities associated with increased mortality in humans, including aging, diabetes, and chronic diseases (2).

A potential disadvantage of our model is that the lung disease that develops following infection with $MERS_{MA}$ may rely upon species-specific mutations arising from selective pressures in the new host. Such selective pressures may not recapitulate all aspects of the human infection. For example, the mutations that arose in the S protein during in vivo serial passage have not been reported in human disease isolates although they are in S domains that show variability among human isolates (75, 76). Our findings suggest that these variable human isolates should be evaluated for distinct host-cell protease dependencies (77). We note that a mouse-adapted SARS-CoV (MA15) that evolved after 15 serial passages in BALB/c mice contained six nucleotide substitutions in five gene products: ORF1a (nsp5 and 9), ORF1b (nsp13), and the S and M proteins (74, 78). A combination of these genetic changes was required to cause virulence. Additional studies are needed to investigate the contributions of individual $MERS_{MA}$ mutations to the lethal phenotype.

Conclusions

The emergence of MERS in 2012 represents the latest example of the zoonotic transmission of a CoV from animal hosts to humans. It is a virtual certainty that other examples of zoonotically transmitted CoV infections will occur in the future. The availability of a small animal model of MERS with a severe disease phenotype provides a tool for the evaluation of novel vaccine strategies, especially in determining the immunopathological consequences of any intervention. Additionally, future studies of the viral mutations associated with mouse adaptation may provide new insights into the virological determinants of severe disease that occur with evolution in a host.

Materials and Methods

All animal studies were approved by the Animal Care and Use Committee of the University of Iowa. Detailed information is provided in *SI Appendix, SI Materials and Methods*.

Generation of Mice with Humanized Exons 10–12 of the Mouse *Dpp4* Gene. A congenic C57BL/6 mouse with mouse *Dpp4* exons 10–12 replaced with the human *DPP4* codons was generated by Taconic Biosciences. This change in exon coding sequence allowed the modified mouse gene product to display amino acids required for virus binding (18–20). The targeting strategy was based on National Center for Biotechnology Information transcripts NM_010074_3 (mouse) and NM_001935_3 (human). The targeting vector was generated using BAC clones from the mouse C57BL/6J RPCIB-731 and human RPCIB-753 BAC libraries. Mouse genomic sequence from codon I264 in exon 10 to codon V340 in exon 12 was replaced with its human counterpart. Positive selection markers were flanked by FRT [neomycin resistance (NeoR)] and F3 [puromycin resistance (PuroR)] sites and inserted into intron 9 and intron 12, respectively. The remaining recombination sites were located in nonconserved regions of the genome. *SI Appendix*, Fig. S1 shows the gene targeting strategy used to generate the human DPP4 knockin mice. Further details on the generation of the model are provided in *SI Appendix, SI Materials and Methods*.

Infection of hDPP4 KI Mice with MERS-CoV. The EMC/2012 strain of MERS-CoV (passage 8, designated MERS-CoV) was provided by Bart Haagmans and Ron Fouchier, Erasmus Medical Center, Rotterdam, The Netherlands. Virus was propagated and titered by plaque assay on Vero 81 cells. This tissue culture amplified virus was termed EMC/Vero. Human DPP4 KI mice were anesthetized with ketamine/xylazine (87.5 mg/kg ketamine/12.5 mg/kg xylazine) and infected intranasally with MERS-CoV in 50 μL DMEM. Infected mice were examined daily and weights recorded. The majority of infections were performed in young, 6- to 8-wk-old mice. Selected experiments were performed in adult mice as noted in *Results* and figure legends. Noninfected littermates served as controls. All MERS-CoV work was conducted in a Biosafety level 3 (BSL3) laboratory.

Virus Titers. Tissues were aseptically removed and dissociated in 1× PBS using a manual homogenizer. Tissue homogenates were centrifuged and supernatants removed. Samples were titered on Vero 81 cells as reported (48).

Extraction of Total RNA and Quantitative RT-PCR. Mouse organs were homogenized in TRIzol and total RNA isolated using the Direct-zol RNA MiniPrep kit (Zymo Research). A DNase treatment step was included. Two hundred nanograms of total RNA was used as a template for first-strand cDNA. The resulting cDNA was subjected to amplification of selected genes by real-time quantitative PCR using Power SYBR Green PCR Master Mix (Applied Biosystems). Average values from duplicates of each gene were used to calculate the relative abundance of transcripts normalized to hypoxanthine guanine phosphoribosyl transferase and presented as $2^{-\Delta CT}$. The primers used were previously reported (32).

Mouse-Adapted MERS-CoV. To develop a model of severe disease, we serially passaged MERS-CoV (EMC/Vero) in hDPP4-KI mice. Two mice were given 10^5 pfu of virus intranasally. Two days later, mice were killed, lungs homogenized in PBS, 50 μL of clarified lung homogenate was administered to two hDPP4-KI mice intranasally, and the process was repeated. Tissue homogenates were saved at each passage.

To obtain a single plaque of a mouse-adapted variant of MERS-CoV, a monolayer of Vero 81 cells in six-well plates was infected with serially diluted virus for 1 h and overlaid by medium containing 1% low-melting-point agarose. Three days after incubation, a single plaque was picked using a sterile Pasteur pipette and transferred into 500 μL DMEM. The isolated plaques were then freeze thawed to release the viral particles from agarose and applied to Huh7 cells to propagate viruses.

Huh7 and Vero 81 cells were grown in DMEM with 10% FBS and 1% penicillin/streptomycin (PS). Calu-3 cells were grown in MEM with 20% FBS and 1% PS. Cells in 24-well plates were infected with indicated MERS-CoV at a multiplicity of infection (MOI) of 0.1. After 1 h of virus adsorption at 37 °C, the virus inocula were removed, the cells were washed with PBS, and new medium was added. At 18–24 h.p.i., virus replication was determined by titrating infectious virus from supernatants on Vero 81 cells.

Histology and Immunohistochemistry. Lungs were prepared for histological examination and for immunohistochemistry for virus antigen and cellular markers after fixation in 10% formalin and embedding in paraffin. For routine histology, tissue sections (~4 μm each) were stained with hematoxylin and eosin. To detect virus N-protein antigen, sections were incubated with a mouse polyclonal antibody [generated by immunizing mice to the MERS-CoV N protein with a virus replicon particles-N vector (48) (1:3,000 dilution)], incubated with a biotinylated anti-mouse secondary antibody, followed by sequential incubation with streptavidin–horseradish peroxidase conjugate (Vectastain ABC kit, Vector Laboratories) and 3,3′-diaminobenzidine (DAB) (Vector Laboratories). Immunolocalization of DPP4 in mouse lung was adapted from previous work (24). Briefly, primary Ab used was a rabbit polyclonal (1:400, PA1-8455; Pierce) and this was followed by a commercial secondary kit (Envision Rabbit, DAKO). DAB was the chromogen and slides were counterstained with Harris hematoxylin. Tissues were evaluated by board certified veterinary pathologists and scored using a postexamination masking method (79). At least five mice (male and female) were analyzed per time point and per experimental condition.

Evans Blue Dye Extravasation. To sedate mice, 1% Evans Blue in 1× PBS was retroorbitally instilled. Thirty minutes postinstillation, mice were killed. PBS (1×) was perfused through the right ventricle, followed by 10% formalin perfusion. Lungs were excised and photographed.

Peripheral Blood Smears. Blood was collected retroorbitally and transferred to a blood collection tube containing EDTA to prevent clotting. Blood smears were produced using the traditional manual method, allowed to dry, and stained with Diff-Quik (Siemens Healthcare Diagnostics) or with modified Wright's stain.

Cell Surface Staining for Flow Cytometry. Mice were killed on 4 d.p.i. and the lungs perfused via the right ventricle with 10 mL PBS. Lung tissues were minced and digested in HBSS buffer containing 2% FCS, 25 mM Hepes, 1 mg/mL Collagenase D (Roche), and 0.1 mg/mL DNase (Roche) for 30 min at room temperature. For surface staining, 5×10^5 cells were blocked with 1 μg anti-CD16/32 antibody and surface stained with the indicated antibodies at 4 °C. Cells were then fixed using Cytofix solution (BD Biosciences). For surface/intracellular staining, cells were incubated with fluorochrome-labeled antibodies specific for mouse: FITC or PECy7-anti-CD45 (30-F11), PE or FITC anti-Ly6G (1A8), PE/PerCp-Cy5.5 anti-Ly6C (AL-21 or HK1.4), PE or V450 anti-CD11b (M1/70), APC anti-F4/80

(BM8), V450 anti-CD11c (N418), APC-CD69 (H1.2F3), APC anti-CD80 (16-10A1), APC-CD3 (145-2C11), FITC anti-CD4 (RM4-5), APC anti-CD8α (53-6.7), PE-CD19 (1D3), PE-Cy7-NKp46 (29A1.4), and PerCp-Cy5.5 anti-IA/IE (M5/114.15.2). Antibodies were procured from BD Biosciences or eBiosciences.

MERS-CoV Genome Sequencing and Assembly. Viral RNA was isolated from producer cell supernatants using a QIAamp Viral RNA MiniKit (Qiagen) according to manufacturer specifications. Viral cDNA was generated using SuperScript III reverse transcriptase and a random hexamer priming approach. Specifically, 11 μL of total RNA was added to 1 μL of FR26RV-N, 1 μL of 10 mM dNTP mix, 4 μL of 5× First Strand Buffer, 1 μL of 0.1 M DTT, 1 μL of RNaseOUT, and 1 μL of SuperScript III Reverse Transcriptase. Further details of library production, sequencing, and genome assembly are provided in *SI Appendix, SI Materials and Methods*.

Generation of Recombinant MERS-CoV by Reverse Genetics. We used reverse genetics to introduce the $MERS_{MA}$ S-protein mutations into an infectious MERS-CoV bacterial artificial chromosome (pBAC-$MERS^{FL}$). The BAC system was developed by Enjuanes and colleagues (50, 51) to generate a EMC/2012 recombinant MERS-CoV and modified by Perlman and colleagues (80). We verified proper construction of the recombinant complete BAC by Sanger sequencing. The full-length BAC cDNA clone was transfected into Huh7 cells to rescue the recombinant virus. Plaque-purified MERS-CoV was amplified to develop stocks.

Statistical Analysis. Student's *t* tests, ANOVA with Dunn's multiple comparison test, or Mann–Whitney rank sum test were used to analyze differences in mean values between groups unless otherwise specified. Results are expressed as mean ± SE. *P* values of ≤0.05 were considered significant.

ACKNOWLEDGMENTS. We thank Luis Enjuanes for providing the bacterial artificial chromosome (pBAC-$MERS^{FL}$) and Jennifer Bartlett and Sateesh Krishnamurthy for their careful review of the manuscript. This work is supported by the National Institutes of Health (NIH) Grant P01 AI060699; and the Cell Morphology Core and Pathology Core, which are partially supported by the Center for Gene Therapy for Cystic Fibrosis (NIH Grant P30 DK-54759) and the Cystic Fibrosis Foundation. P.B.M. is supported by the Roy J. Carver Charitable Trust.

1. Zaki AM, van Boheemen S, Bestebroer TM, Osterhaus AD, Fouchier RA (2012) Isolation of a novel coronavirus from a man with pneumonia in Saudi Arabia. *N Engl J Med* 367:1814–1820.
2. Zumla A, Hui DS, Perlman S (2015) Middle East respiratory syndrome. *Lancet* 386: 995–1007.
3. Yusof MF, et al. (2015) Prevalence of Middle East respiratory syndrome coronavirus (MERS-CoV) in dromedary camels in Abu Dhabi Emirate, United Arab Emirates. *Virus Genes* 50:509–513.
4. Chan RW, et al. (2014) Tropism and replication of Middle East respiratory syndrome coronavirus from dromedary camels in the human respiratory tract: An in-vitro and ex-vivo study. *Lancet Respir Med* 2:813–822.
5. Wernery U, et al. (2015) Acute Middle East respiratory syndrome coronavirus infection in livestock dromedaries, Dubai, 2014. *Emerg Infect Dis* 21:1019–1022.
6. Azhar EI, et al. (2014) Evidence for camel-to-human transmission of MERS coronavirus. *N Engl J Med* 370:2499–2505.
7. Assiri A, et al.; KSA MERS-CoV Investigation Team (2013) Hospital outbreak of Middle East respiratory syndrome coronavirus. *N Engl J Med* 369:407–416.
8. Perlman S, McCray PB, Jr (2013) Person-to-person spread of the MERS coronavirus: An evolving picture. *N Engl J Med* 369:466–467.
9. Breban R, Riou J, Fontanet A (2013) Interhuman transmissibility of Middle East respiratory syndrome coronavirus: Estimation of pandemic risk. *Lancet* 382:694–699.
10. Kucharski AJ, Althaus CL (2015) The role of superspreading in Middle East respiratory syndrome coronavirus (MERS-CoV) transmission. *Euro Surveill* 20:14–18.
11. Memish ZA, Assiri AM, Al-Tawfiq JA (2014) Middle East respiratory syndrome coronavirus (MERS-CoV) viral shedding in the respiratory tract: An observational analysis with infection control implications. *Int J Infect Dis* 29:307–308.
12. Memish ZA, Zumla AI, Al-Hakeem RF, Al-Rabeeah AA, Stephens GM (2013) Family cluster of Middle East respiratory syndrome coronavirus infections. *N Engl J Med* 368:2487–2494.
13. Memish ZA, et al. (2014) Middle East respiratory syndrome coronavirus disease in children. *Pediatr Infect Dis J* 33:904–906.
14. Madani TA (2014) Case definition and management of patients with MERS coronavirus in Saudi Arabia. *Lancet Infect Dis* 14:911–913.
15. Hui DS, Perlman S, Zumla A (2015) Spread of MERS to South Korea and China. *Lancet Respir Med* 3:509–510.
16. Ng DL, et al. (2016) Clinicopathologic, immunohistochemical, and ultrastructural findings of a fatal case of Middle East respiratory syndrome coronavirus infection in the United Arab Emirates, April 2014. *Am J Pathol* 186:652–658.
17. Raj VS, et al. (2013) Dipeptidyl peptidase 4 is a functional receptor for the emerging human coronavirus-EMC. *Nature* 495:251–254.
18. Lu G, et al. (2013) Molecular basis of binding between novel human coronavirus MERS-CoV and its receptor CD26. *Nature* 500:227–231.
19. Wang N, et al. (2013) Structure of MERS-CoV spike receptor-binding domain complexed with human receptor DPP4. *Cell Res* 23:986–993.
20. Barlan A, et al. (2014) Receptor variation and susceptibility to Middle East respiratory syndrome coronavirus infection. *J Virol* 88:4953–4961.
21. Cockrell AS, et al. (2014) Mouse dipeptidyl peptidase 4 is not a functional receptor for Middle East respiratory syndrome coronavirus infection. *J Virol* 88:5195–5199.
22. Song W, et al. (2014) Identification of residues on human receptor DPP4 critical for MERS-CoV binding and entry. *Virology* 471–473:49–53.
23. van Doremalen N, et al. (2014) Host species restriction of Middle East respiratory syndrome coronavirus through its receptor, dipeptidyl peptidase 4. *J Virol* 88:9220–9232.
24. Meyerholz DK, Lambertz AM, McCray PB, Jr (2016) Dipeptidyl peptidase 4 distribution in the human respiratory tract: Implications for the Middle East respiratory syndrome. *Am J Pathol* 186:78–86.
25. Widagdo W, et al. (2016) Differential expression of the Middle East respiratory syndrome coronavirus receptor in the upper respiratory tracts of humans and dromedary camels. *J Virol* 90:4838–4842.
26. Poon LL, et al. (2005) Recurrent mutations associated with isolation and passage of SARS coronavirus in cells from non-human primates. *J Med Virol* 76:435–440.
27. Durai P, Batool M, Shah M, Choi S (2015) Middle East respiratory syndrome coronavirus: Transmission, virology and therapeutic targeting to aid in outbreak control. *Exp Mol Med* 47:e181.
28. Kim ES, et al. (2016) Clinical progression and cytokine profiles of Middle East respiratory syndrome coronavirus infection. *J Korean Med Sci* 31:1717–1725.
29. Kim SY, et al. (2016) Viral RNA in blood as indicator of severe outcome in Middle East respiratory syndrome coronavirus infection. *Emerg Infect Dis* 22:1813–1816.
30. Falzarano D, et al. (2014) Infection with MERS-CoV causes lethal pneumonia in the common marmoset. *PLoS Pathog* 10:e1004250.
31. de Wit E, et al. (2013) Middle East respiratory syndrome coronavirus (MERS-CoV) causes transient lower respiratory tract infection in rhesus macaques. *Proc Natl Acad Sci USA* 110:16598–16603.
32. Li K, et al. (2016) Middle East respiratory syndrome coronavirus causes multiple organ damage and lethal disease in mice transgenic for human dipeptidyl peptidase 4. *J Infect Dis* 213:712–722.
33. Agrawal AS, et al. (2015) Generation of a transgenic mouse model of Middle East respiratory syndrome coronavirus infection and disease. *J Virol* 89:3659–3670.
34. Selinger C, et al. (2014) Cytokine systems approach demonstrates differences in innate and pro-inflammatory host responses between genetically distinct MERS-CoV isolates. *BMC Genomics* 15:1161–1176.
35. Scheuplein VA, et al. (2015) High secretion of interferons by human plasmacytoid dendritic cells upon recognition of Middle East respiratory syndrome coronavirus. *J Virol* 89:3859–3869.
36. Zhou J, et al. (2014) Active replication of Middle East respiratory syndrome coronavirus and aberrant induction of inflammatory cytokines and chemokines in human macrophages: Implications for pathogenesis. *J Infect Dis* 209:1331–1342.
37. Chu H, et al. (2014) Productive replication of Middle East respiratory syndrome coronavirus in monocyte-derived dendritic cells modulates innate immune response. *Virology* 454-455:197–205.
38. Franks TJ, et al. (2003) Lung pathology of severe acute respiratory syndrome (SARS): A study of 8 autopsy cases from Singapore. *Hum Pathol* 34:743–748.
39. Hwang DM, et al. (2005) Pulmonary pathology of severe acute respiratory syndrome in Toronto. *Mod Pathol* 18:1–10.
40. Zhao G, et al. (2015) Multi-organ damage in human dipeptidyl peptidase 4 transgenic mice infected with Middle East respiratory syndrome-coronavirus. *PLoS One* 10:e0145561.
41. van den Brand JM, Smits SL, Haagmans BL (2015) Pathogenesis of Middle East respiratory syndrome coronavirus. *J Pathol* 235:175–184.
42. van Boheemen S, et al. (2012) Genomic characterization of a newly discovered coronavirus associated with acute respiratory distress syndrome in humans. *MBio* 3:e00473-12.
43. Hulswit RJ, de Haan CA, Bosch BJ (2016) Coronavirus spike protein and tropism changes. *Adv Virus Res* 96:29–57.
44. Li F (2016) Structure, function, and evolution of coronavirus spike proteins. *Annu Rev Virol* 3:237–261.
45. Scobey T, et al. (2013) Reverse genetics with a full-length infectious cDNA of the Middle East respiratory syndrome coronavirus. *Proc Natl Acad Sci USA* 110:16157–16162.
46. Park JE, et al. (2016) Proteolytic processing of Middle East respiratory syndrome coronavirus spikes expands virus tropism. *Proc Natl Acad Sci USA* 113:12262–12267.
47. Rosenberger CM, et al. (2014) Characterization of innate responses to influenza virus infection in a novel lung type I epithelial cell model. *J Gen Virol* 95:350–362.
48. Zhao J, et al. (2014) Rapid generation of a mouse model for Middle East respiratory syndrome. *Proc Natl Acad Sci USA* 111:4970–4975.
49. Shirato K, Kanou K, Kawase M, Matsuyama S (2016) Clinical isolates of human coronavirus 229E bypass the endosome for cell entry. *J Virol* 91:e01387-16.
50. Almazán F, et al. (2013) Engineering a replication-competent, propagation-defective Middle East respiratory syndrome coronavirus as a vaccine candidate. *MBio* 4:e00650-13.
51. Almazán F, Márquez-Jurado S, Nogales A, Enjuanes L (2015) Engineering infectious cDNAs of coronavirus as bacterial artificial chromosomes. *Methods Mol Biol* 1282:135–152.
52. Coleman CM, Matthews KL, Goicochea L, Frieman MB (2014) Wild-type and innate immune-deficient mice are not susceptible to the Middle East respiratory syndrome coronavirus. *J Gen Virol* 95:408–412.

53. Raj VS, et al. (2014) Adenosine deaminase acts as a natural antagonist for dipeptidyl peptidase 4-mediated entry of the Middle East respiratory syndrome coronavirus. *J Virol* 88:1834–1838.
54. de Wit E, et al. (2013) The Middle East respiratory syndrome coronavirus (MERS-CoV) does not replicate in Syrian hamsters. *PLoS One* 8:e69127.
55. Munster VJ, de Wit E, Feldmann H (2013) Pneumonia from human coronavirus in a macaque model. *N Engl J Med* 368:1560–1562.
56. Haagmans BL, et al. (2015) Asymptomatic Middle East respiratory syndrome coronavirus infection in rabbits. *J Virol* 89:6131–6135.
57. Adney DR, et al. (2014) Replication and shedding of MERS-CoV in upper respiratory tract of inoculated dromedary camels. *Emerg Infect Dis* 20:1999–2005.
58. Johnson RF, et al. (2015) Intratracheal exposure of common marmosets to MERS-CoV Jordan-n3/2012 or MERS-CoV EMC/2012 isolates does not result in lethal disease. *Virology* 485:422–430.
59. Tao X, et al. (2015) Characterization and demonstration of the value of a lethal mouse model of Middle East respiratory syndrome coronavirus infection and disease. *J Virol* 90:57–67.
60. Pascal KE, et al. (2015) Pre- and postexposure efficacy of fully human antibodies against Spike protein in a novel humanized mouse model of MERS-CoV infection. *Proc Natl Acad Sci USA* 112:8738–8743.
61. Coleman CM, et al. (2016) CD8+ T cells and macrophages regulate pathogenesis in a mouse model of MERS-CoV disease. *J Virol* 91:e01825-16.
62. Cockrell AS, et al. (2016) A mouse model for MERS coronavirus-induced acute respiratory distress syndrome. *Nat Microbiol* 2:16226.
63. Chan RW, et al. (2013) Tropism of and innate immune responses to the novel human betacoronavirus lineage C virus in human ex vivo respiratory organ cultures. *J Virol* 87:6604–6614.
64. Hocke AC, et al. (2013) Emerging human middle East respiratory syndrome coronavirus causes widespread infection and alveolar damage in human lungs. *Am J Respir Crit Care Med* 188:882–886.
65. Channappanavar R, et al. (2016) Dysregulated type I interferon and inflammatory monocyte-macrophage responses cause lethal pneumonia in SARS-CoV-infected mice. *Cell Host Microbe* 19:181–193.
66. Cameron MJ, et al.; Canadian SARS Research Network (2007) Interferon-mediated immunopathological events are associated with atypical innate and adaptive immune responses in patients with severe acute respiratory syndrome. *J Virol* 81:8692–8706.
67. Kobasa D, et al. (2007) Aberrant innate immune response in lethal infection of macaques with the 1918 influenza virus. *Nature* 445:319–323.
68. de Jong MD, et al. (2006) Fatal outcome of human influenza A (H5N1) is associated with high viral load and hypercytokinemia. *Nat Med* 12:1203–1207.
69. Menachery VD, et al. (2014) Pathogenic influenza viruses and coronaviruses utilize similar and contrasting approaches to control interferon-stimulated gene responses. *MBio* 5:e01174–e14.
70. Jiang Y, et al. (2005) Characterization of cytokine/chemokine profiles of severe acute respiratory syndrome. *Am J Respir Crit Care Med* 171:850–857.
71. Tang NL, et al. (2005) Early enhanced expression of interferon-inducible protein-10 (CXCL-10) and other chemokines predicts adverse outcome in severe acute respiratory syndrome. *Clin Chem* 51:2333–2340.
72. Shulla A, et al. (2011) A transmembrane serine protease is linked to the severe acute respiratory syndrome coronavirus receptor and activates virus entry. *J Virol* 85:873–882.
73. Shirato K, Kawase M, Matsuyama S (2013) Middle East respiratory syndrome coronavirus infection mediated by the transmembrane serine protease TMPRSS2. *J Virol* 87: 12552–12561.
74. Roberts A, et al. (2007) A mouse-adapted SARS-coronavirus causes disease and mortality in BALB/c mice. *PLoS Pathog* 3:e5.
75. Cotten M, et al. (2014) Spread, circulation, and evolution of the Middle East respiratory syndrome coronavirus. *MBio* 5:e01062-13.
76. Kim Y, et al. (2016) Spread of mutant Middle East respiratory syndrome coronavirus with reduced affinity to human CD26 during the South Korean outbreak. *MBio* 7:e00019.
77. Millet JK, et al. (2016) A camel-derived MERS-CoV with a variant spike protein cleavage site and distinct fusion activation properties. *Emerg Microbes Infect* 5:e126.
78. Frieman M, et al. (2012) Molecular determinants of severe acute respiratory syndrome coronavirus pathogenesis and virulence in young and aged mouse models of human disease. *J Virol* 86:884–897.
79. Gibson-Corley KN, Olivier AK, Meyerholz DK (2013) Principles for valid histopathologic scoring in research. *Vet Pathol* 50:1007–1015.
80. Fehr AR, et al. (2015) The nsp3 macrodomain promotes virulence in mice with coronavirus-induced encephalitis. *J Virol* 89:1523–1536.